Creating a virtual source inside a medium from reflection data with internal multiples: a stationary-phase analysis

Filippo Broggini and Roel Snieder, Center for Wave Phenomena - Colorado School of Mines;*
Kees Wapenaar, Delft Univ. of Technology

SUMMARY

Seismic interferometry allows one to create a virtual source inside a medium, assuming a receiver is present at the position of the virtual source. We discuss a method that creates a virtual source inside a medium from reflection data measured at the surface, without needing a receiver inside the medium and, hence, going beyond seismic interferometry. In addition to the reflection data, an estimate of the direct arrivals is required. However, no information about the medium is needed. We analyze the proposed method for a simple configuration using physical arguments based on the stationary-phase method and show that the retrieved virtual-source response correctly contains the multiples due to the inhomogeneous medium. The proposed method can serve as a basis for data-driven suppression of internal multiples in seismic imaging.

INTRODUCTION

We propose and discuss a new approach to reconstruct the response to a virtual source inside a medium, going beyond seismic interferometry. Controlled-source interferometric methods (Curtis et al., 2006; Bakulin and Calvert, 2006; Schuster, 2009) allow us to retrieve such a response without the need to know the medium parameters, but these methods require a receiver at the location of the virtual source in the subsurface and assume the medium is surrounded by sources. Our new approach removes the constraint of having a receiver at the virtual source location and is based on an extension of the 1D theory proposed earlier (Broggini et al., 2011, 2012b; Broggini and Snieder, 2012)[1]. They show that, given the reflection response of a 1D layered medium, it is possible to reconstruct the response to a virtual source inside the medium, without having a receiver at the virtual source location and without knowing the medium.

Wapenaar et al. (2011) made a first attempt to generalize the 1D method to 3D media. They used physical arguments to propose an iterative scheme that transforms the reflection response of a 3D medium into the response to a virtual source inside the unknown medium. Apart from the reflection data measured at the surface, our proposed method also requires an estimate of the direct arrivals between the virtual source location and the acquisition surface. These arrivals are a key element of the method, because they specify the location of the virtual source in the subsurface. For this reason, the proposed method is not fully model-independent. However, a model that relates the direct arrival to a virtual source position is simpler than a model that correctly handles the multiples. In the proposed method, the reflection data contributes to the multiple-scattering part of the virtual-source response.

As in seismic interferometry, our goal is to retrieve the response to a virtual source inside an unknown medium, removing the imprint of a complex subsurface. This is helpful in situations where waves have traversed a strongly inhomogeneous overburden (e.g., in subsalt imaging, Sava and Biondi, 2004). Following the work of Wapenaar et al. (2012a)[2], we analyze the iterative scheme for a simple 2D configuration. We use physical arguments based on the stationary-phase method to show that the method converges and allows for the reconstruction of the wavefield originating from the virtual source location.

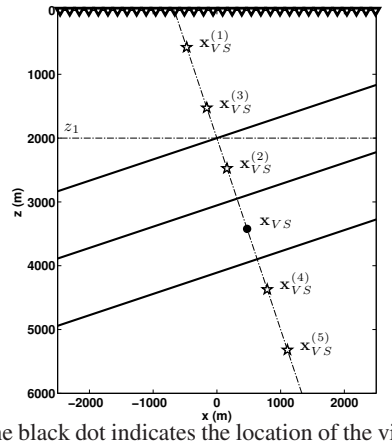

Figure 1: The black dot indicates the location of the virtual source $\mathbf{x}_{VS}$. The star shaped symbols indicate the locations of the mirror images of the virtual source. The triangles denotes the receivers at $z = 0$. The virtual source and its mirror images lie on the line $z = z_1 + x/a$, with $z_1 = 1000$ m and $a = 1/3$.

STATIONARY-PHASE ANALYSIS

We use a geometrical approach to the method of stationary phase to solve the Rayleigh-like integrals, which yield the reflected response to an arbitrary incident field.

Configuration

We consider a configuration of three parallel dipping reflectors in a lossless, constant velocity, variable density medium (Figure 1). We choose a constant velocity medium because the response obeys simple analytical expressions. The proposed iterative scheme is, however, not restricted to constant velocity media. We denote spatial coordinates as $\mathbf{x} = (x, z)$. The acquisition surface is located at $z = 0$ m and is transparent (i.e., the upper halfspace has the same medium parameters as the first layer). The first dipping reflector obeys the relation $z = z_1 - ax$ with $z_1 = 2000$ m and $a = 1/3$. The black dot denotes the position of the virtual source, with coordinates $\mathbf{x}_{VS} = (x_{VS}, z_{VS}) = (475, 3425)$ m. The second and third reflector are parallel to the first one, so that all mirror images of the virtual source lie on a line perpendicular to the reflectors. This line obeys the relation $z = z_1 + x/a$. The first, second, and third reflectors cross this line at $\mathbf{x}_1 = (x_1, z_1)$,

[1] Broggini et al., 2012b, submitted to Geophysics.

[2] Wapenaar et al., 2012a, submitted to Geophysical Journal International.

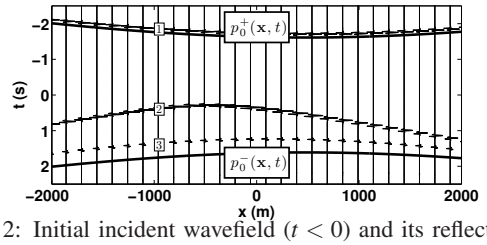

Figure 2: Initial incident wavefield ($t<0$) and its reflection response ($t>0$), both measured at $z=0$. Initial incident wavefield is the time-reversal of the direct arrivals. We show the reflection response only until 2.5 s. The solid black lines denote the time of the direct arrivals and its time-reversed counterpart. These lines are repeated in the subsequent figures.

$\mathbf{x}_2=(x_2,z_2)$, and $\mathbf{x}_3=(x_3,z_3)$, respectively. The velocity of the medium is constant and given by $c=2000$ m/s. The densities in the four layers are $\rho_1=\rho_3=1000$ kg/m^3, $\rho_2=5000$ kg/m^3, and $\rho_4=4000$ kg/m^3, respectively. The reflection coefficients for downgoing waves at the three interfaces are $r_n=(\rho_{n+1}-\rho_n)/(\rho_{n+1}+\rho_n)$, where $n=1,2,3$ denotes the layer. The reflection coefficients for upgoing waves are $-r_n$. The transmission coefficients for downgoing $(+)$ and upgoing $(-)$ waves are $t_n^{\pm}=1\pm r_n$. Since the velocity is constant in this configuration, the reflection and transmission coefficients hold for all the angles of incidence, not only for normal incidence. The large contrast between the density of the layers causes strong multiple reflections.

Primary arrivals

We introduce the Green's function $G(\mathbf{x},\mathbf{x}_S,t)$ as a solution of the wave equation $LG=-\rho\,\delta(\mathbf{x}-\mathbf{x}_S)\frac{\partial\delta(t)}{\partial t}$, with $L=\rho\nabla\cdot(\rho^{-1}\nabla)-c^{-2}\frac{\partial^2}{\partial t^2}$. Defined in this way, the Green's function is the response to an impulsive point source of volume injection rate at $\mathbf{x}_S$ (de Hoop, 1995). Using the Fourier convention $\hat{F}(\omega)=\int_{-\infty}^{+\infty}f(t)\exp(-j\omega t)dt$, the frequency domain Green's function $\hat{G}(\mathbf{x},\mathbf{x}_S,\omega)$ obeys the equation $\hat{L}\hat{G}=-j\omega\rho\,\delta(\mathbf{x}-\mathbf{x}_S)$, with $\hat{L}=\rho\nabla\cdot(\rho^{-1}\nabla)+\omega^2/c^2$. Here j is the imaginary unit, ω denotes the frequency domain. We write $\hat{G}=\hat{G}^d+\hat{G}^s$, where superscripts d and s stand for direct and scattered waves, respectively. As mentioned in the introduction, we need an estimate of the direct arrivals. For the constant velocity model of Figure 1, the high-frequency approximation of the Fourier transform of the direct Green's function $G^d(\mathbf{x},\mathbf{x}_{VS},t)$ is given by $\hat{G}^d(\mathbf{x},\mathbf{x}_{VS},\omega)=t_1^-t_2^-\rho_3\hat{G}_0^d(\mathbf{x},\mathbf{x}_{VS},\omega)$, with

$$\hat{G}_0^d(\mathbf{x},\mathbf{x}_{VS},\omega)=j\omega\frac{\exp\{-j(\omega|\mathbf{x}-\mathbf{x}_{VS}|/c+\mu\pi/4)\}}{\sqrt{8\pi|\omega||\mathbf{x}-\mathbf{x}_{VS}|/c}},\qquad(1)$$

with $\mu=\mathrm{sign}(\omega)$ (Snieder, 2004). The event with label 1 in Figure 2 shows the time-reversed version of the direct arrivals $G^d(\mathbf{x},\mathbf{x}_{VS},t)*s(t)$, where $s(t)$ is a Ricker wavelet with a central frequency of 20 Hz. It is essential that $s(t)$ is zero phase.

Reflection response

To retrieve the virtual-source response $G(\mathbf{x},\mathbf{x}_{VS},t)$, we need the reflection response at the surface $R(\mathbf{x}_R,\mathbf{x}_S,t)*s(t)$, in addition to an estimate of the direct arrivals. We assumed that the acquisition surface is transparent, hence the reflection response does not include any surface-related multiples. For this purpose, $R(\mathbf{x}_R,\mathbf{x}_S,t)*s(t)$ can be obtained from reflection data measured at $z=0$ after surface-related multiple elimination (Verschuur et al., 1992). Following Bleistein (1984), the reflection response can be derived

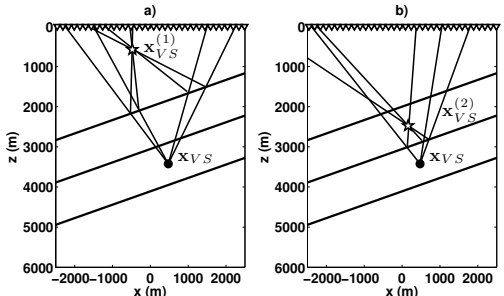

Figure 3: Analysis of the response of the first and second reflectors to the initial incident wavefield $p_0^+(\mathbf{x},t)$. Stationary rays for different receivers. (a) The response of the first reflector seems to originate from $\mathbf{x}_{VS}^{(1)}$. (b) The response of the second reflector seems to originate from $\mathbf{x}_{VS}^{(2)}$.

from a Rayleigh-type integral:

$$\hat{p}^-(\mathbf{x}_R,\omega)=\int_{-\infty}^{\infty}\frac{2}{j\omega\rho_1}\left[\frac{\partial\hat{G}^s(\mathbf{x}_R,\mathbf{x},\omega)}{\partial z}\hat{p}^+(\mathbf{x},\omega)\right]_{z=0}dx,\quad(2)$$

where $\hat{p}^+$ and $\hat{p}^-$ are the Fourier transform of the downgoing and upgoing wavefields, respectively. Hence, in the frequency domain, we define the reflection response in terms of the scattered Green's function $\hat{G}^s$ via

$$\hat{R}(\mathbf{x}_R,\mathbf{x}_S,\omega)\hat{s}(\omega)=\frac{2}{j\omega\rho_1}\frac{\partial\hat{G}^s(\mathbf{x}_R,\mathbf{x}_S,\omega)}{\partial z_S}\hat{s}(\omega),\qquad(3)$$

for $z_R=z_S=0$ and after multiplying both sides by the spectrum of the source wavelet $s(t)$.

Initiating the iterative process

We define the initial incident downgoing wavefield at $z=0$ as the time-reversed version of the direct arrivals at the recording surface excited by the virtual source $\mathbf{x}_{VS}$. Hence, the initial wavefield is $p_0^+(\mathbf{x},t)=G^d(\mathbf{x},\mathbf{x}_{VS},-t)*s(t)$ and is shown in Figure 2 with the label 1. The subscript 0 of $p_0^+(\mathbf{x},t)$ indicates the initial wavefield (or the 0th iteration). In Figure 2, we also define two traveltime curves, indicated by the solid black lines. The upper curve is taken directly after the initial incident wavefield $p_0^+(\mathbf{x},t)$ and the lower curve is defined as the time-reversal of the upper curve. These two curves allow us to define a window function

$$\begin{aligned}&w(\mathbf{x},t)=1\quad\text{between the solid black lines of Figure 2}\\&w(\mathbf{x},t)=0\quad\text{elsewhere.}\end{aligned}\qquad(4)$$

This window function is a key component of the iterative scheme. The reflected upgoing wavefield $p_0^-(\mathbf{x},t)$ is obtained by convolving the downgoing incident wavefield $p_0^+(\mathbf{x},t)$ with the deconvolved reflection response and integrating over the source positions:

$$p_0^-(\mathbf{x}_R,t)=\int_{-\infty}^{\infty}\left[R(\mathbf{x}_R,\mathbf{x},t)*p_0^+(\mathbf{x},t)\right]_{z=0}dx,\qquad(5)$$

for $z_R=0$. Equation (5) is the time-domain version of the Rayleigh integral described by equation (2). We discuss and solve this integral with geometrical arguments based on the method of stationary phase (a detailed mathematical proof is given by Wapenaar et al., 2012a). Figure 3 shows a number of stationary rays for different receiver positions. These rays are said to be stationary because the rays of the incident field (converging in $\mathbf{x}_{VS}$) and of the reflec-

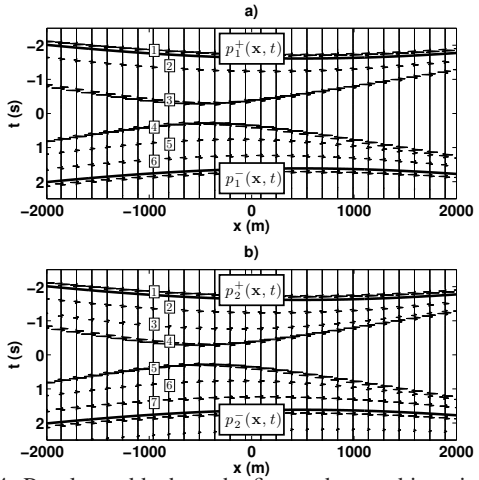

Figure 4: Panel a and b show the first and second iteration of the incident wavefield ($t<0$) and its reflection response ($t>0$), respectively (both measured at $z=0$). The numbers identify events in the total field. We show the reflection response only until 2.5 s.

tion response (for the first reflector) have the same direction (see the appendix of Wapenaar et al., 2010). With simple geometrical arguments it follows that these rays cross each other at the mirror image of the virtual source with respect to the first reflector, i.e., at $\mathbf{x}_{VS}^{(1)}$. The traveltimes of the convolution product are given by the length of the rays from $\mathbf{x}_{VS}^{(1)}$ to the surface, divided by the velocity. Hence, it is as if the response of the first reflector to the initial incident field originates from a source at $\mathbf{x}_{VS}^{(1)}$. This response is thus equal to $r_1 G^d(\mathbf{x}_R,\mathbf{x}_{VS}^{(1)},t)*s(t)$ and is shown as the event with label 2 in Figure 2. Following similar stationary-phase arguments, the response of the second reflector to the initial downgoing field apparently originates from a mirror image of the virtual source with respect of the second reflector, i.e., at $\mathbf{x}_{VS}^{(2)}$. This response is equal to $t_1^- r_2 t_1^+ G^d(\mathbf{x}_R,\mathbf{x}_{VS}^{(2)},t)*s(t)$, see the event with label 3 in Figure 2. However, the multiple reflected responses to the initial incident field also apparently originate from mirror images of the virtual source, all located along the line $z=z_1+x/a$, see Figure 1. We derived these responses with the method of stationary phase, hence they are free of artifacts.

The iterative process

We now discuss an iterative scheme, which uses the (k-1)th iteration of the reflection response $p_{k-1}^-(\mathbf{x},t)$ to create the kth iteration of the incident field $p_k^+(\mathbf{x},t)$. The objective is to iteratively update the incident field in such a way that, within the upper and lower solid black lines shown in Figure 2, the field is anti-symmetric in time. The meaning of this criterion will be evident in the next section, where we show how to reconstruct $G(\mathbf{x},\mathbf{x}_{VS},t)$. The method requires a combination of time reversal and windowing and the kth iteration of the incident field is defined by

$$p_k^+(\mathbf{x},t)=p_0^+(\mathbf{x},t)-w(\mathbf{x},t)p_{k-1}^-(\mathbf{x},-t),\quad \text{for } \mathbf{x} \text{ at } z=0, \quad (6)$$

where the time window $w(\mathbf{x},t)$ is defined by equation (4). The reflection response is then obtained using equation (5), that we rewrite here as

$$p_k^-(\mathbf{x}_R,t)=\int_{-\infty}^{\infty}\left[R(\mathbf{x}_R,\mathbf{x},t)*p_k^+(\mathbf{x},t)\right]_{z=0}dx, \quad (7)$$

for $\mathbf{x}$ and $\mathbf{x}_R$ at $z=0$. The first and second iteration of the incident and reflected fields are shown in Figures 4a and 4b, respectively. The events of $p_2^+(\mathbf{x},t)$ labeled 2,3,4 in Figure 4b correspond to the events of $p_1^-(\mathbf{x},t)$ labeled 6,5,4 in Figure 4a (time-reversed and multiplied by -1). For this particular configuration, the kth iteration of the incident field (for $k>2$) is similar to $p_2^+(\mathbf{x},t)$ and it is composed by four events, as show in Figure 4b for $t<0$. The events labeled 1 and 4 remain unchanged in the iterative process. The other two events (labeled 2 and 3) correspond to $-A_k^{(2)}G^d(\mathbf{x}_R,\mathbf{x}_{VS}^{(2)},-t)*s(t)$ and $-A_k^{(3)}G^d(\mathbf{x}_R,\mathbf{x}_{VS}^{(3)},-t)*s(t)$, respectively. The coefficient $A_k^{(2)}$ varies at each iteration and is equal to the partial sum of the geometric series $c+cx+cx^2+cx^3+cx^4+\cdots+cx^k$ where $c=t_1^+r_2t_1^-t_2^-t_1^-$ and $x=r_1^2$. The sum of the series converges, because $x<1$, and it yields

$$\sum_{k=0}^{\infty}cx^k=\frac{c}{1-x}=r_2t_2^-t_1^-, \quad (8)$$

where we used that $1-r_1^2=t_1^-t_1^+$. The coefficient of the third event, $A_k^{(3)}$ (labeled 3 in Figure 4b), is equal to $-r_1A_k^{(2)}$ and it converges to $-r_1r_2t_2^-t_1^-$. Figure 5a shows the thirtieth iteration and, within the time window $w(\mathbf{x},t)$, the wavefield is antisymmetric in time. This is the result we predicted when we described the iterative method. The antisymmetry was actually the design criterion for the iterative scheme. This procedure is expected to converge because in each iteration the reflected energy is smaller than the incident energy. We consider the proposed method as a correction scheme that minimizes the energy inside the time window $w(\mathbf{x},t)$.

Wavefield reconstruction from the virtual source

After showing that the method converged to the desired result, we define $p_k(\mathbf{x},t)$ as the superposition of the kth version of the incident and reflected wavefields: $p_k(\mathbf{x},t)=p_k^+(\mathbf{x},t)+p_k^-(\mathbf{x},t)$. Figures 2, 4a, 4b and 5a show $p_k(\mathbf{x},t)$ for $k=0,1,2,$ and 30, respectively. For brevity, we define $p(\mathbf{x},t)=p_{30}(\mathbf{x},t)$. We remind the reader that, within the solid black lines, the total field at $z=0$ is antisymmetric in time and this particular feature was the design criterion for the iterative scheme. Consequently, if we stack the total field and its time-reversed version, i.e., $p(\mathbf{x},t)+p(\mathbf{x},-t)$, all events inside the time window cancel each other, as shown in Figure 5b. Note that $p(\mathbf{x},t)+p(\mathbf{x},-t)$ also obeys the wave equation because we consider a lossless medium. The causal part of this superposition corresponds to $p^-(\mathbf{x},t)+p^+(\mathbf{x},-t)$ and the anti-causal part is equal to $p^+(\mathbf{x},t)+p^-(\mathbf{x},-t)$, as shown in Figure 5b for $t<0$ and $t>0$, respectively. From a physical point of view, time-reversal changes the propagation direction, hence it follows that the causal part propagates upward at $z=0$ and the anti-causal part propagates downward at $z=0$. The first event of the causal part of Figure 5b has the same arrival time of the direct arrival of the response to the virtual source at $\mathbf{x}_{VS}$. If we combine this last observation with the fact that the causal part is upward propagating at $z=0$, and that the total field obeys the wave equation in the inhomogeneous medium and is symmetric, it is plausible that the total field in Figure 5b is proportional to $G(\mathbf{x},\mathbf{x}_{VS},t)+G(\mathbf{x},\mathbf{x}_{VS},-t)$. More precisely, we speculate that $G(\mathbf{x},\mathbf{x}_{VS},-t)$ and $G(\mathbf{x},\mathbf{x}_{VS},t)$ are proportional to the anti-causal and causal parts of Figure 5b, respectively. This deduction does not take into account any particular feature of the configuration used in this analysis, hence it should hold for more general situ-

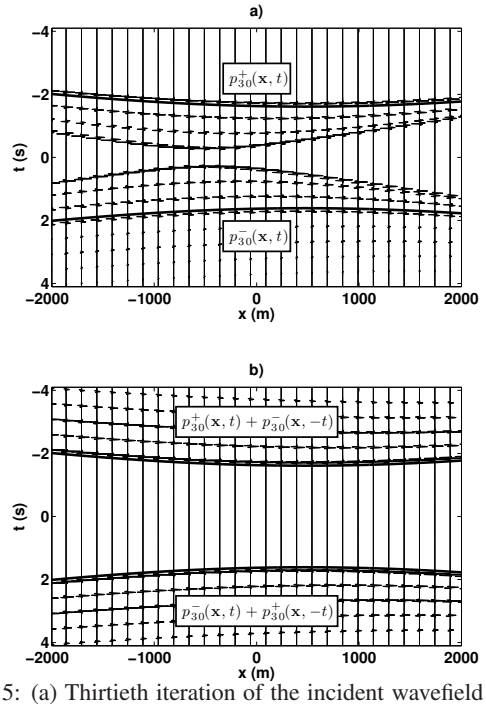

Figure 5: (a) Thirtieth iteration of the incident wavefield ($t<0$) and its reflection response ($t>0$), both measured at $z=0$. Within the solid black lines, the total field is antisymmetric in time and this particular feature was the design criterion for the iterative scheme. (b) Superposition of the total field and its time-reversed version after the method has converged. Here, unlike the previous figures, we show the wavefield for the time interval $-4<t<4$ s.

ations. We will check its validity for the response in Figure 5b. Following the steps that led to the field shown in Figure 5b, we find for the causal part that

$$\begin{aligned} &p^-_{30}(\mathbf{x},t)+p^+_{30}(\mathbf{x},-t)= \qquad (9)\\ &\quad t^+_1t^+_2\Big\{G^d(\mathbf{x},\mathbf{x}_{VS},t)+r_3G^d(\mathbf{x},\mathbf{x}^{(4)}_{VS},t)-\\ &\quad r_2(r_1+r_3)G^d(\mathbf{x},\mathbf{x}^{(5)}_{VS},t)-r_3r_2(r_1+r_3)G^d(\mathbf{x},\mathbf{x}^{(6)}_{VS},t)-\\ &\quad (r_1r_3-r_2^2(r_1+r_3))G^d(\mathbf{x},\mathbf{x}^{(7)}_{VS},t)\ldots\Big\}*s(t), \end{aligned}$$

with the virtual source position and its mirror images shown in Figure 1. For the configuration of Figure 1, this is proportional to the wavefield $G(\mathbf{x},\mathbf{x}_{VS},t)*s(t)$ originated from the virtual source and recorded at the surface (with $t^+_1t^+_2$ as the coefficient of proportionality). The directly modeled response to the virtual source is shown in Figure 6 and it matches the causal part of the field shown in Figure 5b. For the total wavefield we obtain

$$p(\mathbf{x},t)+p(\mathbf{x},-t)=t^+_1t^+_2G_h(\mathbf{x},\mathbf{x}_{VS},t)*s(t), \qquad (10)$$

where $G_h(\mathbf{x},\mathbf{x}_{VS},t)=G(\mathbf{x},\mathbf{x}_{VS},t)+G(\mathbf{x},\mathbf{x}_{VS},-t)$. We note that $G(\mathbf{x},\mathbf{x}_{VS},-t)$ obeys the same wave equation as $G(\mathbf{x},\mathbf{x}_{VS},t)$, i.e., $LG(\mathbf{x},\mathbf{x}_{VS},-t)=-\rho_3\delta(\mathbf{x}-\mathbf{x}_{VS})\frac{\partial\delta(-t)}{\partial(-t)}=\rho_3\delta(\mathbf{x}-\mathbf{x}_{VS})\frac{\partial\delta(t)}{\partial t}$. So, G_h obeys the homogeneous equation $LG_h=-\rho_3\delta(\mathbf{x}-\mathbf{x}_{VS})\frac{\partial\delta(t)}{\partial t}+\rho_3\delta(\mathbf{x}-\mathbf{x}_{VS})\frac{\partial\delta(t)}{\partial t}=0$. This is in agreement with the fact that $p(\mathbf{x},t)+p(\mathbf{x},-t)$ has been constructed without introducing a singularity (i.e., a real source) at $\mathbf{x}_{VS}$. G_h is called the homogeneous Green's function, after Porter (1970) and Oristaglio (1989) (but note that these authors take the difference instead of the sum of the causal and acausal Green's functions because of a different definition of the source in the wave equation).

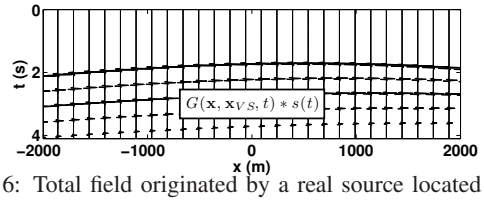

Figure 6: Total field originated by a real source located at $\mathbf{x}_{VS}$, i.e., $G(\mathbf{x},\mathbf{x}_{VS},t)*s(t)$.

CONCLUSIONS

We proposed a generalization to 2D of the model-independent wavefield reconstruction method of Broggini et al. (2011, 2012b). The proposed data driven procedure yields the response to a virtual source and reconstructs correct internal multiples, without needing a receiver at the virtual source location and without needing detailed knowledge of the medium. The method requires (1) the direct arriving wave front at the surface originated from a virtual source in the subsurface, and (2) the reflection impulse responses for all source and receiver positions at the surface. For a simple configuration, the stationary-phase analysis gives insight into the mechanism of the 2D iterative scheme and confirms that the methods converges to the virtual-source response. Following the physical arguments in the previous section, it is plausible that the proposed methodology will also apply to more complex environments. The method will also have its limitations. The effects of a finite acquisition aperture, triplications, head waves, fine-layering, errors in the direct arrivals, etc. need further investigation. A numerical test by one of us with a variable-velocity syncline model shows promising results with respect to the handling of triplications (Broggini et al., 2012a)[3]. Errors in the estimated direct arrivals will cause defocusing and mispositioning of the virtual source (as in standard imaging algorithms). Such errors, however, do not affect the handling of the internal multiples and do not deteriorate their reconstruction, which is handled by the actual medium through the reflection data (that includes all the information about the medium itself). Because the proposed method is non-recursive, the reconstruction of internal multiples will not suffer from error magnification, unlike other imaging methods that aim at internal multiple suppression. Since no actual receivers are needed inside the medium, virtual sources can be created anywhere. The virtual-source responses contain all internal multiples, hence the method could be used as a basis for imaging without internal multiples (Wapenaar et al., 2012b).

ACKNOWLEDGMENTS

This work was supported by the sponsors of the Consortium Project on Seismic Inverse Methods for Complex Structures at the Center for Wave Phenomena and the Netherlands Research Centre for Integrated Solid Earth Science (ISES).

[3]Broggini et al., 2012a, SEG Technical Program Expanded Abstracts, this issue.

REFERENCES

Bakulin, A., and R. Calvert, 2006, The virtual source method: Theory and case study: Geophysics, **71**, SI139–SI150.

Bleistein, N., 1984, Mathematical methods for wave phenomena: Academic Press. Computer science and applied mathematics.

Broggini, F., and R. Snieder, 2012, Connection of scattering principles: a visual and mathematical tour: European Journal of Physics, **33**, 593–613.

Broggini, F., R. Snieder, and K. Wapenaar, 2011, Connection of scattering principles: Focusing the wavefield without source or receiver: SEG Technical Program Expanded Abstracts, **30**, 3845–3850.

———, 2012a, Creating a virtual source inside a medium from reflection data: numerical examples for laterally-varying velocity models, spatially-extended virtual sources, and inaccurate direct arrivals: SEG Technical Program Expanded Abstracts, this issue.

———, 2012b, Focusing the wavefield inside an unknown 1D medium - Beyond seismic interferometry: submitted to Geophysics.

Curtis, A., P. Gerstoft, H. Sato, R. Snieder, and K. Wapenaar, 2006, Seismic interferometry—turning noise into signal: The Leading Edge, **25**, 1082–1092.

de Hoop, A. T., 1995, Handbook of radiation and scattering of waves: Academic Press, London.

Oristaglio, M., 1989, An inverse scattering formula that uses all the data: Inverse Problems, **5**, 1097–1105.

Porter, R. P., 1970, Diffraction-limited, scalar image formation with holograms of arbitrary shape: Journal of the Optical Society of America, **60**, 1051–1059.

Sava, P., and B. Biondi, 2004, Wave-equation migration velocity analysis - II: Subsalt imaging example: Geophysical Prospecting, **52**, 607–623.

Schuster, G. T., 2009, Seismic Interferometry: Cambridge University Press.

Snieder, R., 2004, A Guided Tour of Mathematical Methods for the Physical Sciences, 2nd ed.: Cambridge University Press.

Verschuur, D. J., A. J. Berkhout, and C. P. A. Wapenaar, 1992, Adaptive surface-related multiple elimination: Geophysics, **57**, 1166–1177.

Wapenaar, K., F. Broggini, and R. Snieder, 2011, A proposal for model-independent 3D wave field reconstruction from reflection data: SEG Technical Program Expanded Abstracts, **30**, 3788–3792.

———, 2012a, Creating a virtual source inside a medium from reflection data: a stationary-phase analysis: submitted to Geophysical Journal International, **189**.

Wapenaar, K., D. Draganov, R. Snieder, X. Campman, and A. Verdel, 2010, Tutorial on seismic interferometry: Part 1 - Basic principles and applications: Geophysics, **75**, 75A195–75A209.

Wapenaar, K., J. Thorbecke, J. van der Neut, F. Broggini, and R. Snieder, 2012b, Creating virtual sources inside an unknown medium from reflection data: a new approach to internal multiple elimination: EAGE Expanded Abstracts.